

Review

# Improving Photocatalytic Performance Using Nanopillars and Micropillars

Jessica L. Waite, Julianna Hunt and Haifeng Ji \* 

Department of Chemistry, Drexel University, Philadelphia, PA 19104, USA; jlw478@drexel.edu (J.L.W.); julianna.louise.hunt@drexel.edu (J.H.)

\* Correspondence: hj56@drexel.edu; Tel.: +1-215-895-2562; Fax: +1-215-895-1265

**Abstract:** A recent research emphasis has been placed on the development of highly crystallized nanostructures as a useful technology for many photocatalytic applications. With the unique construction of semiconductor transition metal oxide nanostructures in the form of nanopillars—artificially designed pillar-shaped structures grouped together in lattice-type arrays—the surface area for photocatalytic potential is increased and further enhanced through the introduction of dopants. This short review summarizes the work on improving the efficiency of photocatalyst nanopillars through increased surface area and doping within the applications of water splitting, removal of organic pollutants from the environment, photoswitching, soot oxidation, and photothermalization.

**Keywords:** nanopillars; photocatalyst



**Citation:** Waite, J.L.; Hunt, J.; Ji, H. Improving Photocatalytic Performance Using Nanopillars and Micropillars. *Materials* **2021**, *14*, 299. <https://doi.org/10.3390/ma14020299>

Received: 29 October 2020

Accepted: 29 December 2020

Published: 8 January 2021

**Publisher's Note:** MDPI stays neutral with regard to jurisdictional claims in published maps and institutional affiliations.



**Copyright:** © 2021 by the authors. Licensee MDPI, Basel, Switzerland. This article is an open access article distributed under the terms and conditions of the Creative Commons Attribution (CC BY) license (<https://creativecommons.org/licenses/by/4.0/>).

## 1. Introduction

Nanostructures of semiconductive photocatalysts, such as titanium dioxide (TiO<sub>2</sub>), including nanopillars, quantum nanowires, and thin films have been developed for visible light-driven photocatalytic reactions [1]. Metal nanoparticles have been proven to enhance photocatalytic activity due to their surface plasmon resonance properties [2]. Due to the large bandgap of TiO<sub>2</sub>, as well as the low recombination rate of electron–hole pairs and large potential for energy conversion observed by TiO<sub>2</sub> nanocomposite semiconductors, the wavelength of solar absorption window within these materials is broadened, thus increasing photoactivity [3].

Increased surface area in these nanostructures demonstrated enhanced photoactivity [4]. Specific surface area has shown to be increased by introducing transitional metal oxide nanostructure “guests” doped into the host’s interlayers [5]. With increased surface area, TiO<sub>2</sub> nanopillars are subject to doping and sensitizing with semiconductors, transition metal ions, and nonmetals with enhancing sustainable energy pathways such as the photoelectrochemical splitting of water into hydrogen, soot oxidation, and conversion of atmospheric carbon dioxide into hydrocarbon structures. A catalyst having a high specific surface area can increase the reaction rate due to an increased number of organic molecules on the surface of the catalyst [5]. Concerning photocatalyst, an increased surface area may create more active sites available for water and hydroxyl absorption, trapping photogenerated charges for radicals to promote photodegradation [5]. These new active sites lead to the formation of other active structures.

Other transition metal oxides are used for water splitting and decomposition of organic pollutants due to their commercial benefits and low environmental risks [6]. Reactive hydroxyl radicals on the surface of titanium dioxide are the key to the catalyst’s water purification abilities. As UV light enters the material, electron–hole pairs are photogenerated to interact in redox reactions at the surface of the catalyst [6]. The electron–hole pairs can dissociate into hydrogen and hydroxyl radicals, which are then used for the decomposition of pollutant levels in water [7].

The efforts of various groups have been compiled for analysis to determine how the photocatalytic efficiency of the nanomaterials has been enhanced. An emphasis is put on the results rather than the synthesis, allowing the reader to see the direct effect of each group's experimental work.

## 2. Nanopillars for Water Splitting—Improving the Efficiency due to Doping Silicon or Titanium Dioxide Nanopillars

Water splitting using solar energy is of particular interest. Water splitting processes have been used to produce reusable energy sources such as molecular oxygen and hydrogen, contributing to the decline of carbon dioxide emission and dependence on fossil fuels [8]. This photocatalytic process has, therefore, been the subject of many studies due to its valuable products, which can also be produced using photoelectrode in oxygen or hydrogen-evolution reactions. In an electrode used for water splitting, the location of optical absorbance is wherever the electron hole charge carrier can contribute to the surface reactions [4]. The surface, therefore, controls the intake of photons being absorbed on the semiconductor electrode; increased light available to the surface provides more photons to the electrode. Nanopillared surfaces provide such a capability.

Several transition metal oxides have been used for water splitting purposed due to their commercial benefits and low environmental risks [9]. By attaching one-dimensional nanostructures to the surface of such oxides, it is possible to increase the light absorbance by increase surface area.

### 2.1. Titanium Dioxide—TiO<sub>2</sub>

Transitional metal oxides are commonly used as photocatalysts. Titanium dioxide (TiO<sub>2</sub>) has been discovered as an efficient photocatalyst in the reduction in water to produce H<sub>2</sub> evolution in a very stable, nontoxic, and cost-efficient way. However, the material proves to be problematic in the visible light range and show poor productivity due to a wide band gaps around ~3 eV [10]. Thus, doping TiO<sub>2</sub> with other materials, such as semiconductors; transition metal ions; and nonmetals, have been studied to improve the photocatalytic efficiency, as introducing other materials with smaller band gaps will improve the productivity of the large band gap material.

One of the most effective approaches to extending the titanium dioxide light absorption range is the doping of titanium dioxide with nonmetal elements. Xing et al. reported a one-step thermal protection method to synthesize an S-doped porous anatase titanium dioxide nanopillar, which maintains its anatase structure up to 700 °C, resulting in high levels of crystallinity and photocatalytic activity in the solar region [11]. The band gap of the pure TiO<sub>2</sub> sample was found to be 3.2 eV, greater than the band gaps of the four S-doped samples at differing calcination temperature, T-500, T-600, T-700, and T-800, which have band gaps at 2.85, 2.92, 3.00, and 3.16, respectively. This suggests narrowing of the bandgap due to the introduction of S particles, which promotes visible-light absorption and enhanced photon utilization. The H<sub>2</sub> evolution of the S-doped sample reached 163.9 μmolh<sup>-1</sup>g<sup>-1</sup> for sample T-700, suggesting that a calcination temperature of 700 °C is most efficient for hydrogen evolution. Samples T-500, T-600, and T-800 had H<sub>2</sub> evolution values of 35.09, 77.39, and 44.79 μmolh<sup>-1</sup>g<sup>-1</sup>, respectively. There is no report of hydrogen evolution values for a pure TiO<sub>2</sub> samples, but it can be implied the study is focused on how calcination temperature of TiO<sub>2</sub> samples doped with S affects photocatalytic activity.

Qu et al. [11] reported a one-pot method without surfactant for the synthesis of silver-titanium dioxide (Ag-TiO<sub>2</sub>) heterojunction nanopillars for the conversion of solar energy to H<sub>2</sub>. Such nanopillars provide a heterogeneous junction interface when light-harvesting semiconductors and cocatalyst are paired, which improves electron charge transfer and separation, allowing for the conception of a high-performance photocatalyst. The enhancement of light production at this interface is attributed to the surface plasmon resonance properties of metal nanoparticles, such as silver, within the synthesized metal-semiconductor photocatalyst. Three different samples were produced having differing molar ratios of Ag to TiO<sub>2</sub>. An increase in Ag to TiO<sub>2</sub> ratio shows increased intensity,

suggesting higher amounts of Ag particles increase the production of Ag-TiO<sub>2</sub> composites; an Ag to TiO<sub>2</sub> molar ratio of 20:1 is the most efficient. This AT-20 (Ag-TiO<sub>2</sub> at a molar ratio of 20) shows a higher efficiency that is 72.1  $\mu\text{molh}^{-1}$  greater than that of AT-10 and AT-40, whose irradiation values under visible light were 38.2 and 44.2  $\mu\text{molh}^{-1}$ , respectively. Compared to a planar sample of Pt-loaded TiO<sub>2</sub> having irradiation values of 5.4  $\mu\text{molh}^{-1}$ , all three samples showed greater photocatalytic performance due to the junctions between Ag cocatalyst and TiO<sub>2</sub> semiconductor. Therefore, AT-20 was the most efficient in H<sub>2</sub> production, while the planar sample showed the lowest efficiency.

The photoelectrochemical (PEC) efficiency of the oxides may be increased by means of manipulation of the oxide heterostructure, which, in turn, separates the electron-hole pairs and floods the electron-hole pair deficiencies in the material. The photogenerated electron-hole pairs in the 1D shell contribute to the increased photoelectric features when their charges show a moderate separation. TiO<sub>2</sub> has also been used as a doping material into other photoactive semiconductor, such as 1D silicon nanopillars (SiNP), to improve the effectiveness of the Si. Pavlenko et al. tested the effectiveness of a silicon nanopillar doped or coated with TiO<sub>2</sub> and zinc oxide (ZnO) heterostructures [8]. Four samples of silicon nanopillars having different metal oxide heterostructure core shells were produced: a silicon nanopillar with TiO<sub>2</sub> coating (SiNP/TiO<sub>2</sub>), a silicon nanopillar with ZnO coating (SiNP/ZnO), a silicon nanopillar with both TiO<sub>2</sub> and ZnO coating (SiNP/TiO<sub>2</sub>/ZnO), and a planar comparison sample of SiNP. The result showed that nanopillars with 1D core shells, specifically containing silicon and both TiO<sub>2</sub> and ZnO, have the ability to improve photocurrent densities up to 60 and 4 times higher than SiNP/TiO<sub>2</sub> and SiNP/ZnO at the water-splitting potential of 1.23 V vs. RHE (0.63 V vs. Ag/AgCl), respectively. This is due to the photoelectric properties that pertain to the mixture of these oxides. The SiNP/TiO<sub>2</sub>/ZnO sample showed to have higher efficiency in charge separation and transfer. When comparing the plane SiNP sample to those doped with ZnO, TiO<sub>2</sub>, or both metal oxides, there is a significant increase in intensity of the GIXRD spectra when doping is present, changing intensity from >100 a.u. to approximately 1200 a.u. when doped with both metals.

## 2.2. Hematite—Fe<sub>2</sub>O<sub>3</sub>

To optimize the light intake, materials with smaller band gaps that can more efficiently utilize the UV-VIS spectra are used for water splitting. Hematite ( $\alpha$ -Fe<sub>2</sub>O<sub>3</sub>) is an n-type semiconductor with various uses. Fe<sub>2</sub>O<sub>3</sub> is commonly used for photoanode in water splitting due to its commercial benefits, but, more importantly, it has a low band gap of 2.2 eV [4] and solar-to-hydrogen efficiency of ~17%, thus hematite works in the visible light range. However, due to hematite's poor minority charge carrier mobility, the short hole diffusion length and high electron-hole recombination rate of hematite restrict its possibility for application within the photoelectrochemical cell. The production of hematite nanostructures may be the answer to this problem.

Liao et al. reported a rapid dehydration strategy involving the quasi-topotactic transformation of FeOOH nanorods to porous Fe<sub>2</sub>O<sub>3</sub> pillars, capable of photoelectrochemical water oxidation. The implementation of Fe<sub>2</sub>O<sub>3</sub> nanorods would reduce the distance needed for hole diffusion and overcome the poor charge transport limitation [9]. This strategy is accomplished by directly dehydrating the FeOOH nanorods in a high-temperature furnace (Figure 1). Two samples were produced, including a sample of nanorod a conventional temperature sample, C-Fe<sub>2</sub>O<sub>3</sub> (the planar Fe<sub>2</sub>O<sub>3</sub> sample with conventional temperature-rising technique) and a Rapid Dehydration sample, RD-Fe<sub>2</sub>O<sub>3</sub>. Photocurrent density was found to have improved by 270%, with values of 2.0 mA/cm<sup>2</sup> (1.23 V vs. RHE) and 3.5 mA/cm<sup>2</sup> (1.71 V vs. photoanodes RHE) for the RD-Fe<sub>2</sub>O<sub>3</sub> photoanode, compared to the conventional C-Fe<sub>2</sub>O<sub>3</sub> sample having photocurrent density values of 0.75 mA/cm<sup>2</sup> (1.23 V vs. RHE) and 1.48 mA/cm<sup>2</sup> (1.71 V vs. photoanodes RHE). This can be accredited to the lowered charge-carrier recombination (electron-hole pair recombination rate) due to single crystalline nanopillars, increase light harvesting ability due to the production of longer nanopillars,

and a porous structure that shortens the distance between bulk material and the interface between electrode and electrolyte.

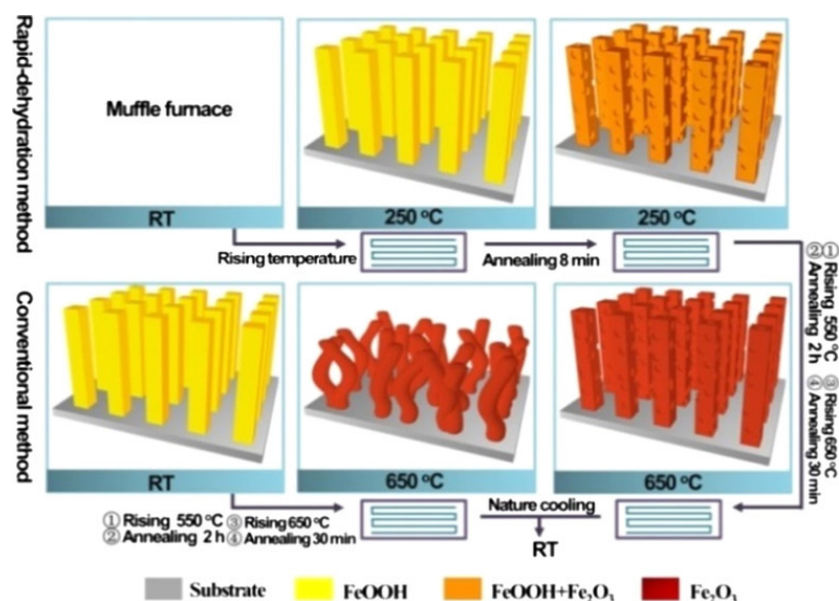


**Figure 1.** Schematic illustration of the preparation of conventional C-Fe<sub>2</sub>O<sub>3</sub> compared to rapid dehydration RD-Fe<sub>2</sub>O<sub>3</sub>. (Adapted from [9] Figure 1, with permissions from ACS).

Gao et al. [4] created samples of gold photoanodes having Au nanopillar arrays (AuNPAs) for use as electrical contacts and plasmonic couplers with hopes of increasing the photoelectric activity of the Hematite iron (III) oxide photoanodes. Synthesis of the samples can be seen in Figure 2. An increase in surface area of 30% in the electrode of the AuNPAs is observed compared to the planar sample. A photocurrent enhancement of about 40% was observed in the patterned AuNPA sample over the planar sample at 1.5 V vs. RHE (reversible hydrogen electrode), and it can be increased to 50% by increasing the thickness of the AuNPAs.

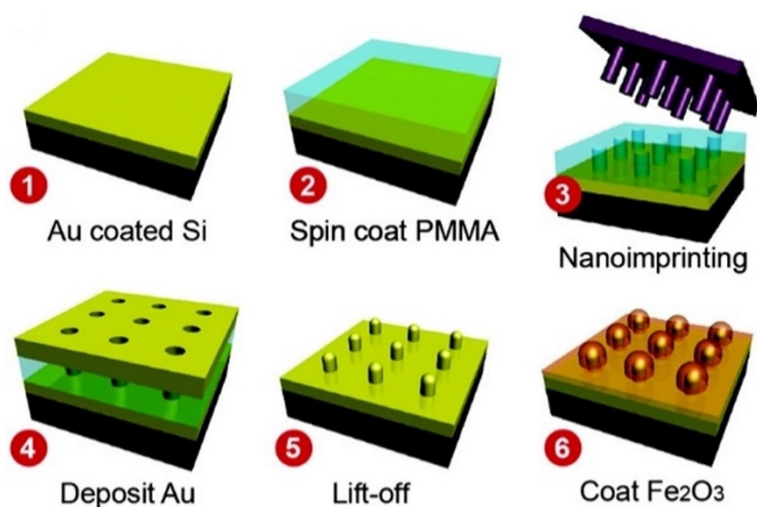


**Figure 2.** Silicon semiconductor is coated with gold. The nanoprinting technique is then displayed to show how the material is coated with Au nanopillar arrays (AuNPAs) and then layered with Fe<sub>2</sub>O<sub>3</sub>. (Adapted from [4] Figure 1, with permissions from ACS).

Ahn et al. investigated the applicability of the hematite iron oxide species in water splitting performance by synthesizing a hematite and Ti-doped SiO<sub>x</sub> passivation layer struc-

ture (Ti-SiO<sub>x</sub>/np-Fe<sub>2</sub>O<sub>3</sub>) to be compared to a simple Ti-Fe<sub>2</sub>O<sub>3</sub> sample. The thin passivation layer of Ti-doped of amorphous SiO<sub>x</sub> was synthesized in situ by hydrothermal/annealing processes to induce nanopores and increase photoelectrochemical performance [12]. The surface area of the Ti-(SiO<sub>x</sub>/np-Fe<sub>2</sub>O<sub>3</sub>) sample increased by 2.5 times compared to the simple Ti-Fe<sub>2</sub>O<sub>3</sub> sample. The Ti-(SiO<sub>x</sub>/np-SiO<sub>x</sub>) sample showed a photocurrent density of 2.44 mA cm<sup>-2</sup> at 1.23 V<sub>RHE</sub>, a 200% enhancement of the simple Ti-Fe<sub>2</sub>O<sub>3</sub> sample having a photocurrent density of 1.23 mA cm<sup>-2</sup> at 1.01 V<sub>RHE</sub>. The high photocurrent density results obtained for the Ti-doped substrate are attributed to the protected surface states and the increased surface area because of its nanosized pore characterization.

Table 1 compares the performance of the nanomaterials and their planar counterparts for water splitting.

**Table 1.** The performance of the nanomaterials and their planar counterparts.

| Nanomaterial for Enhanced Photocatalytic Performance   | Planar Comparison Sample  | Improved Photocatalysis Compared to Planar Sample  |
|--|---|--|
| S-doped TiO <sub>2</sub> with hydrogenation evolution value of 163.9 μmolh <sup>-1</sup> g <sup>-1</sup> at a calcination temperature of 700 °C. [10]            | No quantitative comparison to pure TiO <sub>2</sub> , but when compared to S-doped samples calcinated at 500, 600, and 800 °C, H <sub>2</sub> evolution values are significantly lower: 35.09, 77.39, and 44.79 μmolh <sup>-1</sup> g <sup>-1</sup> . | N/A  |
| AT-20: 72.1 μmolh <sup>-1</sup> greater<br>AT-10: 38.2 μmolh <sup>-1</sup><br>AT-40: 44.2 μmolh <sup>-1</sup> [11]   | Pt-loaded TiO <sub>2</sub> : irradiation values of 5.4 μmolh <sup>-1</sup>  | Raman spectra values increase from 147.7 cm <sup>-1</sup> for TiO <sub>2</sub> comparison to 152.7 cm <sup>-1</sup> for Ag-TiO <sub>2</sub> nanopillars.   |
| SiNP/TiO <sub>2</sub><br>SiNP/ZnO<br>SiNP/TiO <sub>2</sub> /ZnO [8]  | SiNP  | SiNP/TiO <sub>2</sub> /ZnO shows photocurrent densities 60 times higher than SiNP/TiO <sub>2</sub> and 4 times higher than SiNP/ZnO. An increase in intensity from 100 to 1200 a.u. is found compared to the planar SiNP sample. |
| Rapid dehydration sample RD-Fe <sub>2</sub> O <sub>3</sub> : 2.0 mA/cm <sup>2</sup> (1.23 V vs. RHE) and 3.5 mA/cm <sup>2</sup> (1.71 V vs. photoanodes RHE) [9] | Conventional temperature sample C-Fe <sub>2</sub> O <sub>3</sub> : 0.75 mA/cm <sup>2</sup> (1.23 V vs. RHE) and 1.48 mA/cm <sup>2</sup> 157 (1.71 V vs. photoanodes RHE).   | Photocurrent density improved by 270%.   |
| Patterned AuNPAs [4]   | Planar Au substrate   | 30% surface area increase; 50% photocurrent enhancement over solar spectrum.   |
| Ti-doped SiO <sub>x</sub> photocurrent density of 2.44 mA cm <sup>-2</sup> at 1.23 V <sub>RHE</sub> , [12]   | Ti-Fe <sub>2</sub> O <sub>3</sub> : photocurrent density of 1.23 mA cm <sup>-2</sup> at 1.01 V <sub>RHE</sub>   | Surface area enhancement of 2.5 times compared to planar sample, 200% photocurrent density enhancement.  |

### 3. Nanopillars for Removing Organic Pollutants

Reactive hydroxyl radicals on the surface of photocatalysts such as TiO<sub>2</sub> are the key to the catalyst's pollutants-removing abilities. As UV light enters the material, electron-hole pairs are photogenerated to perform redox reactions at the surface of the catalyst. The electron-hole pairs can create or generate hydrogen and hydroxyl radicals, which are then used for the decomposition of pollutant levels in water.

#### 3.1. Improving the Efficiency of Oxides due to Larger Surface Area

To produce thin film materials with more capable photocatalytic abilities, it has been questioned how the photocatalytic properties of oxides may be manipulated towards into a porous or nanopillared morphology. The synthesis of materials exhibiting characteristics such as a nanopillars structure, mesoporous network, efficient adsorption capacity, and increased surface area are of high interest in the field of photocatalysis.



The application of nonsilica containing materials onto electric, photonic, and magnetic nanodevices suggests a solution for increased photocatalytic properties in place of previously used materials. Titanium dioxide is commonly used for water purification due to its commercial benefits as well as low corrosion rates. The common anatase phase (3.2 eV) of titanium dioxide shows the highest rates of photocatalytic activity due to high electron functioning. The morphology and pore/particle size have significant influence over the photocatalytic processes of the TiO<sub>2</sub>. A reduction in the size of the TiO<sub>2</sub> photocatalyst allows for greater surface area for redox reactions to take place.

Kimura et al. investigated porous anatase thin films produced due to the deformation of 3D mesostructures to achieve a better understanding of the photocatalytic properties based on crystallization and porosity [13]. The thin film samples being investigated included a 3D hexagonal mesostructured titania thin film prepared with a precursor solution, a 3D mesostructured film, and a commercial anatase film. Degradation of methylene blue (MB) was observed in each sample. Crystallinity is seen completely in both hexagonal and mesostructured samples, therefore, surface area and pore size are investigated to determine photocatalytic abilities.  $S_{\text{eff-MB}}$  values show information about photocatalytic abilities relative to effective surface area of the MB.  $S_{\text{eff-MB}}$  value of the hexagonal structure was reported at 0.0095 mol/cm<sup>3</sup>, compared to mesostructure's value of 0.0148 mol/cm<sup>3</sup>, and the commercial anatase sample's value of 0.0016 mol/cm<sup>3</sup>. The commercial comparison sample showed significantly decreased photocatalytic abilities due to low porosity. Porous films of fully crystallized anatase nanoparticles show enhanced photocatalytic abilities and the deformation of 3D mesostructures allow for proper adjustment of intercrystallite mesospaces. This method can be utilized to produce electrodes with increased porous structures in nanodevices as well as the production of enhanced photocatalyst systems.

Tin (IV) oxide (SnO<sub>2</sub>) is a conducting oxide with lower conduction band than TiO<sub>2</sub>. Cheng et al. reported that the photocatalytic properties can be enhanced by incorporating a SnO<sub>2</sub>/TiO<sub>2</sub> core-shell nanopillar-array structure that utilizes both the heterojunction and high surface of SnO<sub>2</sub>/TiO<sub>2</sub> [3]. The resulting products were tested with methylene blue (MB) irradiation. TiO<sub>2</sub> films with and without a SnO<sub>2</sub> interlayer were produced, having decay constants of 0.094 and 0.065 h<sup>-1</sup>. It was found that SnO<sub>2</sub> nanopillars act as a sink for electron carriers released from TiO<sub>2</sub> and increases the lifetime of hole carriers for methylene blue (MB) degradation. The photocatalytic properties were improved by 180% and 300% for sample with and without SnO<sub>2</sub> interlayer when compared to a planar TiO<sub>2</sub>.

### 3.2. Degradation of Organic Pollutants due to Photocatalytically Enhanced TiO<sub>2</sub> Nanostructures

The prevalence of unwanted organic micropollutants in pharmaceuticals, drinking water, and personal care products raises a serious concern to the environment and the public health domain. Some of them are highly toxic chemical species even at very low concentrations. The exploration of heterojunction nanopillars has been accomplished through the addition of sulfide, nitride, and oxide cocatalysts onto TiO<sub>2</sub> semiconductor surface to create a light-harvesting interface. By enhancing periodical texture through a micropillar array of TiO<sub>2</sub> on flat surface materials, as well as exploring structural imperfections through band gap structure alteration at boundary defect sites, the photoactivity of TiO<sub>2</sub> semiconductor nanostructures improves.

Steroidal hormones, specifically those known as endocrine disrupting chemicals (EDCs) are highly dangerous to the environment due to threatening levels of estrogen and low ability to be biologically decomposed. These toxic chemicals may damage human puberty rates and spermatozoa levels as they enter the ecosystem through runoff and excretion, whether it be direct or due to commercial use. More specifically, an EDC known as 17 $\alpha$ -Ethinylestradiol, or EE2, is one such dangerous hormone used in birth control pills and hormone therapies. Water ways and sewage lines are contaminated with the pollutant, leading to increased exposure. Commonly used semiconductor TiO<sub>2</sub> offers a way for heterogeneous photocatalytic processes to clean the pollutants from water systems. Electron-hole pairs of the titanium dioxide allow for the absorption of pollutants through

oxidation and reduction reactions, resulting in a superoxide radical,  $O_2^-$ , and hydroxyl radical,  $OH\cdot$  ( $E^0 = 2.80$  V). In water systems where EE2 was present, the hydroxyl radical removed the pollutant by 92%. Photocatalytic degradation of indicators such as Alizarin Yellow further indicate the strength of the photocatalytic abilities [8]. Recently, two thin film samples were prepared to investigate how nanopillars surface affect the degradation of EE2: a titanium dioxide nanopillar thin film produced with PEG filler (S2), and a thin film produced without PEG filler (S1). The sample using only UV light is used as the “planar” reference sample. Percent degradation at a pH of 6 shows about 16% removal using UV light, whereas samples S1 and S2 have degradation percentages around 20% and 30%, respectively. Compared to solely UV light treatment, samples S1 and S2 proved to be efficient treatments for organic pollutant water cleansing.

At the semiconductor surface level, the lattice defects influence the electron-transfer processes of semiconductor  $TiO_2$  species and affect the photocatalytic properties of the semiconductor at these interfacial boundary sites through the introduction of dopants. Additionally, altering the band gap structure at boundary defect sites through chemical intervention techniques, such as imidazolium type ionic liquids, allow for more efficient charge transfer routes and an increased oxygen evolution for semiconductor nanowires. Song et al. [14] explored the case of  $TiO_2$  in which the imidazolium ionic liquid semiconductor (liquid–solid) interface is developed as a tuning surface for altering shape and size of  $TiO_2$  nanocrystals into aggregated clusters—this alteration tunes the defect sites at boundary regions and allows for the development of efficient photocatalytic materials. Surface-modified quantum wires (SMoQWs) were observed for photocatalysis as well as the zero-dimensional nanoclustered nanowires (NCNWs) from which they were fabricated. The transition from NCNWs (associated with the  $TiO_2$  rutile phase) to SMoQWs occurs because of nitrogen doping of intercrystalline void spaces (Figure 3). When exposed directly to UV light, the SMoQWs samples had a 15.8% increase in photocatalytic properties compared to NCNWs. The SMoQWs sample showed degradation rates 8 times faster than that of NCNWs. By engineering void defects in crystal structures of  $TiO_2$  nanopillars, low-dimensional quantum material growth from nanoclusters generates heterocoordination sites and enhances photocatalytic performance.

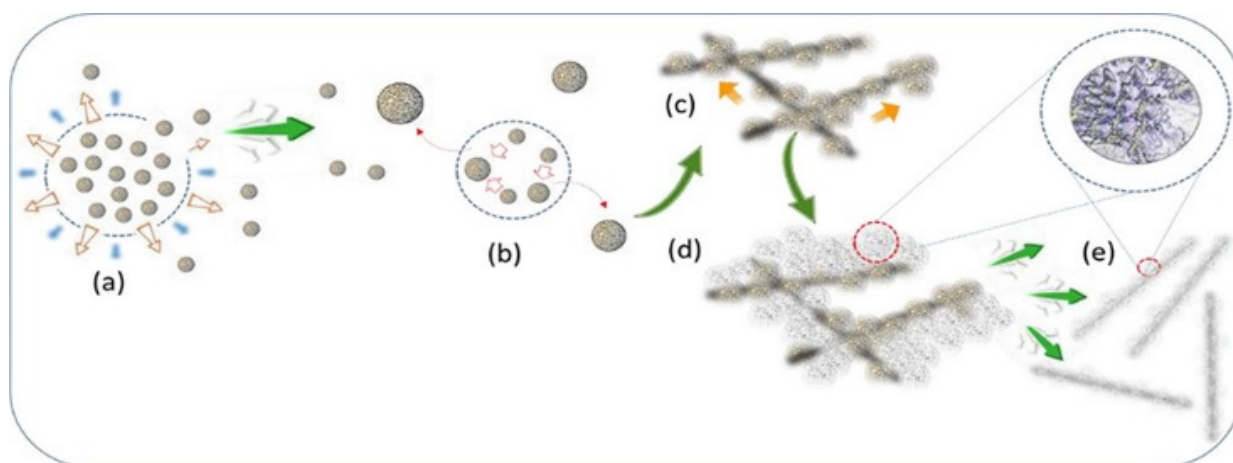


**Figure 3.** Schematic representation showing formation of surface-modified quantum wires (SMoQWs) from nanoclustered nanowires (NCNWs). (a) Centers of nucleation form and (b) assemble into larger particles by the process of coalescence driven by Ostwald ripening and undergo (c) multidirectional growth into NCNWs and (d) removal of high-energy weakly bonded particles to form (e) nanopillars of SMoQWs. (Adapted from [14] Figure 1, with permissions from ACS).

### 3.3. Improving the Efficiency with Decorated $TiO_2$ Nanopillars

The use of  $TiO_2$  as a degradation agent for organic pollutants as well as water splitting is of high interest, as previously mentioned in various studies due to the compound's

photocatalytic properties.  $\text{TiO}_2$  is commonly used for its photocatalytic properties, yet its use is faulted by low quantum yield and low utilization rates of the visible light spectrum (~5%). The deposition of noble metals on  $\text{TiO}_2$  can alter the surface properties of  $\text{TiO}_2$  and inhibit recombination carriers, therefore changing the photocatalytic activity.

Shuang et al. investigated the codecorated Au/Pt noble metal nanoparticles on  $\text{TiO}_2$  vertically aligned nanopillar arrays to measure organic pollutant (dye) degradation [15]. As one quantum size effect approach to enhancing the accessibility of  $\text{TiO}_2$  as a photocatalytic semiconductor,  $\text{TiO}_2$  nanopillar arrays were vertically synthesized on substrates in order to maximize reaction surface area. The metallic nanoparticles were applied through atomic layer deposition, and the  $\text{TiO}_2$  was annealed at three different temperatures to ensure the photocatalytic performance of the nanopillar. In studying the photocatalytic mechanism (Figure 4), the noble metal nanoparticles observe a “hot” electron shift from the surface of the Au to the Pt cocatalyst through the  $\text{TiO}_2$  conduction band. The photoelectrochemical performance and the dye degradation of the vertically aligned nanopillar array were measured at various annealing temperatures; the highest experimental dye degradation efficiency was reported as 75.3% at 300 °C, while the efficiency for Au/Pt– $\text{TiO}_2$  without atomic layer deposition (ALD) was 49.3%. Conclusively, this ALD method for synthesis of Au/Pt– $\text{TiO}_2$  with annealing represents a rational design for the functionality of vertically aligned nanopillars to efficiently maximize solar energy usage for photocatalytic dye degradation of common organic pollutants.

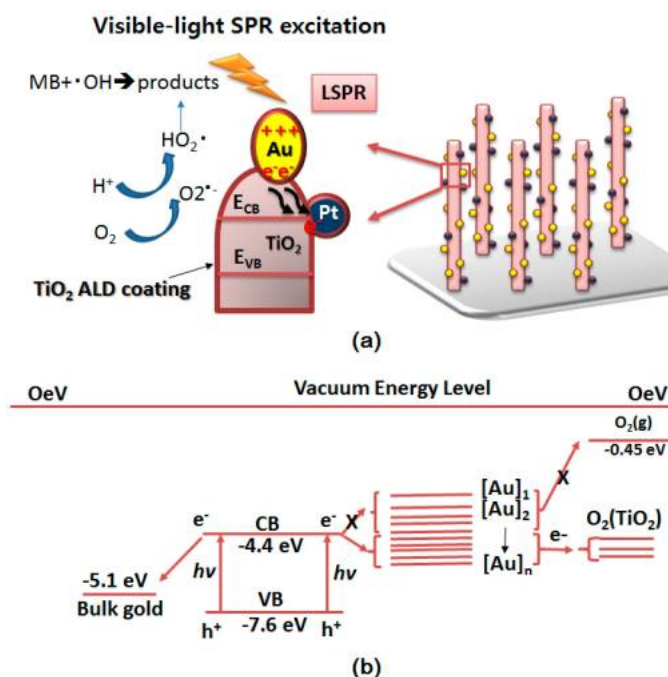


**Figure 4.** (a) The charge transfer process of  $\text{TiO}_2$  ALD/Au/Pt/ $\text{TiO}_2$  NPAs under UV-VIS lights; (b) Fermi level of nanoscale gold particles. (Adapted from [15] Figure 6, with permissions from MDPI’s open access license).

Shuang et al. also introduced Au and Pt nanoparticles (NPs) on  $\text{TiO}_2$  nanopillar arrays (NPAs) to increase the photocatalytic properties of the  $\text{TiO}_2$  for pollutant degradation [2]. In their study, they used metal coupling techniques to improve photocatalysis by the Schottky barrier conduction band (CB) electron trapping and increase electron–hole pair lifetime. The use of metals slows the charge-pair recombination by acting as an electron sink or by trapping electrons on the CB to be transferred to electron acceptors. This study produced four samples of NPs decorated with  $\text{TiO}_2$  composite NPAs: pure  $\text{TiO}_2$  NPAs, Pt– $\text{TiO}_2$  NPAs, Au– $\text{TiO}_2$  NPAs, and Au/Pt– $\text{TiO}_2$  NPAs. The resulting Au/Pt NPs decorated with  $\text{TiO}_2$  composite NPAs show highly enhanced photocatalytic activity for degradation of



methylene orange (MO) and overall photoelectric (PEC) activity in comparison to other NPAs. The photocatalytic efficiency is 21 times greater under UV-VIS light and 13 times higher under visible light than that of pure TiO<sub>2</sub> due to the electron-sink system of Pt and surface plasmon resonance of Au nanopillars.

Standard water treatment systems are unable to rid waterways of such antibiotics pollutants, such as tetracycline, creating a need for oxidation processes including TiO<sub>2</sub> photocatalyst [16]. Tiwari et al. aimed to improve the limited photocatalytic functions of TiO<sub>2</sub> through the doping of noble metal nanoparticles of Au onto the titanium dioxide. These nanoparticles show surface plasmon resonance effect under UV and visible light irradiation and act as cocatalyst in separation of electron-hole pairs, aiding the reactions taking place at the surface of the material. Two samples were produced both containing gold doping with or without a poly(ethylene glycol) (PEG) solid template, known as Au/TiO<sub>2</sub> (A) and Au/TiO<sub>2</sub> (B). Sample (A) was nontemplated without PEG solid, and sample (B) was templated with PEG solid. The tetracycline was mineralized by the photocatalytic degradation under UV-A light ( $\lambda > 330$  nm). Repeated use of the thin films was possible due to its stability. The degradation of the tetracycline pollutant was mainly due to the hydroxyl radicle produced at the valence and the conduction bands of the semiconductor. Results showed that samples containing Au particles show much greater photocatalysis. It is suggested that use of the PEG solid template increases stability and photocatalytic abilities compared to sample (A). In final analysis, the embellishment of noble metals onto titanium dioxide photocatalyst increase the degradation rates of micropollutants in water systems.

Nitrogen dopants have been used to attempt to alter the bandgap of TiO<sub>2</sub> [17]. This study conducted by Jiang et al. hoped to fabricate TiO<sub>2</sub> nanopillar arrays doped with nitrogen that have adjustable bandgaps of varying wavelengths within the visible light range. Ag nanoparticles were also embedded onto TiO<sub>x</sub>N<sub>y</sub> nanopillars by photoreduction in Ag<sup>+</sup> (aq) under irradiation of visible light. TiN films were oxidated to produce TiO<sub>x</sub>N<sub>y</sub>, which was compared to the unoxidized TiN. Photoactivity was tested at different oxidation temperatures. A temperature of 550 °C shows the greatest photocatalytic ability as Rhodamine B (RhB) was degraded >50% and a color change was observed. Incorporation of Ag particles significantly increases photocatalytic properties. The TiO<sub>x</sub>N<sub>y</sub> matrix bandgap was found to be adjustable, and the addition of Ag particles embedded into the matrix enhances the photocatalytic abilities.

Zhang et al. used cesium titanate to produce pillared nanocomposites. Cesium titanate has similar properties to TiO<sub>2</sub> and has a large band gap. Transition metal doping has been used to increase light absorption due to band gap narrowing. The hybridization of two different semiconductors were known to decrease the electron-hole pair recombination probability [5]. The semiconductor guest particles are inserted into the interlayer of the 2D semiconductor host lattice to create a heterojunction structure. Therefore, the samples being investigated included an Fe-doped cesium titanate (having two semiconductors to act as guest particles and a host lattice, Cs<sub>0.68+x</sub>Ti<sub>1.83-x</sub>Fe<sub>x</sub>O<sub>4</sub>) and ZnO pillared doped titanate (only having one semiconductor for band gap narrowing, ZnO/Ti<sub>1.83-x</sub>Fe<sub>x</sub>O<sub>4</sub>). A bare ZnO nanoparticle was used for comparison. The bare ZnO nanoparticles degraded methylene blue (MB) by 4% after a 90-min irradiation. During the same increment of irradiation, the Cs<sub>0.68+x</sub>Ti<sub>1.83-x</sub>Fe<sub>x</sub>O<sub>4</sub> sample degraded 25.8% of MB molecules ( $x = 0.04$ ) and the ZnO/Ti<sub>1.83-x</sub>Fe<sub>x</sub>O<sub>4</sub> sample had a maximum degradation rate of 67.7% ( $x = 0.02$ ). Surface area increased from the cesium sample (1 m<sup>2</sup>/g) to the ZnO nanoparticle (12 m<sup>2</sup>/g) to the ZnO pillared doped titanate (103 m<sup>2</sup>/g). Degradation of MB increased from the ZnO nanoparticle to the Cs<sub>0.68+x</sub>Ti<sub>1.83-x</sub>Fe<sub>x</sub>O<sub>4</sub> sample to the ZnO/Ti<sub>1.83-x</sub>Fe<sub>x</sub>O<sub>4</sub> sample. All the samples were compared to those not containing Fe doping, and it was concluded that iron ions increased the response to the UV range.

### 3.4. Improving the Efficiency with Decorated Hematite Nanopillars

Shuang et al. studied the photocatalytic performance of CdS nanoparticle decorated with hematite nanopillar arrays (CdS NP/ $\alpha$ -Fe<sub>2</sub>O<sub>3</sub> NPAs) and compared that with a pure hematite nanopillar array sample [18]. Electron–hole separation can be achieved using CdS, which has a small bandgap and high absorption rate. Photogenerated electrons from CdS nanoparticles transfer into the hematite to achieve charge-carrier separation. The photocurrent density and degradation efficiency for NPA's with CdS NP and without was about 94% degradation in 75 min vs. 78% dye degradation, respectively. The CdS NP/ $\alpha$ -Fe<sub>2</sub>O<sub>3</sub> NPAs showed increased photocurrent density of 2.0 mAcm<sup>2</sup> at 0.4 V vs. Ag/AgCl. The result showed that heterojunctions of CdS hematite provides efficient solar energy conversion and photocatalysis.

Table 2 compares the performance of the nanopillars and their planar counterparts for removing the organic pollutants.

**Table 2.** The performance of the nanopillars and their planar counterparts.

| Nanopillar for Removing Organic Pollutants   | Comparison Sample                                      | Overall Improved Efficiency Compared to Planar Sample   |
|--|--|---|
| 3D hexagonal mesostructured titania thin film<br>3D mesostructured film<br>[13]  | Commercial anatase film                                | Surface area is compared through Seff-MB values. Values were re-ported as 0.0095, 0.0148, and 0.0016 mol/cm <sup>3</sup> for the hexagonal mesostructured, mesostructured, and commercial samples, respectively.                                  |
| SnO <sub>2</sub> /TiO <sub>2</sub> core-shell nanopillar array<br>[3]  | Flat TiO <sub>2</sub>                                  | 180% (with SnO <sub>2</sub> ) and 300% (without SnO <sub>2</sub> ) enhancement in photocatalytic properties compared to flat TiO <sub>2</sub> .   |
| S2 (with PEG filler)<br>S1 (without PEG filler)<br>[8]   | UV light treatment                                     | UV light shows 16% degradation, 20% for S1, and 30% for S2.   |
| SMoQW (surface-modified quantum wires)<br>[14]   | NCNW (nanoclustered nanowires)                         | 15.8% improvement in photocatalytic performance compared to NCNW  |
| Au/Pt–TiO <sub>2</sub> with atomic layer deposition<br>[15]  | Au/Pt–TiO <sub>2</sub> without atomic layer deposition | Dye degradation rates of 75.3% and 49.3% for samples with and without ALD, respectively.  |
| Au/Pt–TiO <sub>2</sub><br>[2]  | Pure TiO <sub>2</sub> NPA                              | Au/Pt–TiO <sub>2</sub> showed an enhanced photocatalytic efficiency of 21 times greater than that of pure TiO <sub>2</sub> under UV–VIS light, and 13 times greater under visible light.  |
| Au/TiO <sub>2</sub> (A) (nontemplated without PEG solid)<br>Au/TiO <sub>2</sub> (B) (templated with PEG solid)<br>[16]                     | Simple UV-A  | Sample Au/TiO <sub>2</sub> -B maximum percent tetracycline degradation of 68% compared to 41% of the simple UV sample.  |
| Oxidized TiO <sub>x</sub> N <sub>y</sub><br>[17]   | TiN  | Approximately 50% degradation compared to plane TiN.  |
| ZnO/Ti <sub>1.83–x</sub> Fe <sub>x</sub> O <sub>4</sub><br>Cs <sub>0.68+x</sub> Ti <sub>1.83–x</sub> Fe <sub>x</sub> O <sub>4</sub><br>[5] | Bare ZnO   | Bare ZnO degraded MB at 4% efficiency, while Cs <sub>0.68+x</sub> Ti <sub>1.83–x</sub> Fe <sub>x</sub> O <sub>4</sub> had degrading rate of 25.8, and ZnO/Ti <sub>1.83–x</sub> Fe <sub>x</sub> O <sub>4</sub> showed a degradation rate of 67.7%. |
| CdS NP/ $\alpha$ -Fe <sub>2</sub> O <sub>3</sub> NPAs<br>[18]  | Pure hematite NPAs                                     | Dye degradation with and without CdS NP was 94% and 78%, respectively.  |

### 4. Nanopillars for Breaking Organic Chemicals for Analysis

Degradation of organic pollutants can be used in analysis. As an example, drug candidates can often form toxic metabolites. Taking place in the liver, phase I of drug metabolism involves enzymes, which biotransform xenobiotics into polar metabolites. It is in this phase that toxic metabolites are formed and therefore is of particular interest for research. Phase I oxidation reactions can be mimicked or modeled by electrochemistry techniques, such as liquid chromatography and mass spectrometry taking place in an electrochemical cell [19]. To mimic phase I of metabolism of organic compounds, a TiO<sub>2</sub>-

coated microchip was developed using titanium dioxide nanoreactors and UV radiation for production, detection, and identification purposes of metabolites and reaction products. The microchip can be used to produce, detect, and identify photocatalytic reaction products of specific drugs that may mimic phase I of metabolism. The TiO<sub>2</sub> microchip proved to have faster speed and higher sensitivity compared to other *in vitro* models. The microchip model shows greater photocatalysis ability opposed to degradation efficiency. Moreover, 50% of the maximum signal of verapamil metabolites were reached in 2 min. A correlation was found between metabolites found *in vitro* and *in vivo* methods compared to reaction products seen on the microchip. Further information about change in degradation rates and photocurrent density was not given. It was concluded that the titanium dioxide microchip can predict phase I metabolites in the early stages of drug study and can help uncover new drug contenders.

In another work, Temerov et al. explore the liquid flame spray (LFS) technique of TiO<sub>2</sub> nanoparticles onto stainless steel while measuring deviations in photocatalytic activity and comparing the efficiency of flat surface nanostructures to the metal injected molded (MIM) stainless steel array structures [20]. The study reported the increased active surface area of the MIM manufactured micropillar arrays after LFS with TiO<sub>2</sub> on stainless steel, resulting in a higher photocatalytic activity and a resistance to tribological wear (Figure 5). In comparison, the flat surface reference sample lost complete photocatalytic activity as a result of harsh condition exposure; the flat sample reported a low photocatalytic activity of 4.2 ppm/h, while the high density micropillars reported an activity of 15.6 ppm/h. MIM micropillar arrays produced on stainless steel surfaces increase surface area and increase photocatalytic activity after liquid flame spray deposition of titanium dioxide nanoparticles. Decrease in surface area and resulting photocatalytic performance after tribological wear was observed at 100% decrease, 32% decrease, and 16.2% decrease for the sample without micropillars, high-density micropillars, and low-density micropillars, respectively. A mixture of rutile and anatase can show more enhanced photocatalytic activity compared to the singular anatase phase. The incorporation of TiO<sub>2</sub> nanoparticle application to stainless steel micropillars through the LFS technique with MIM microtextures provides a highly photocatalytic and versatile technique for light-harvesting that can withstand mechanical and environmental wear.

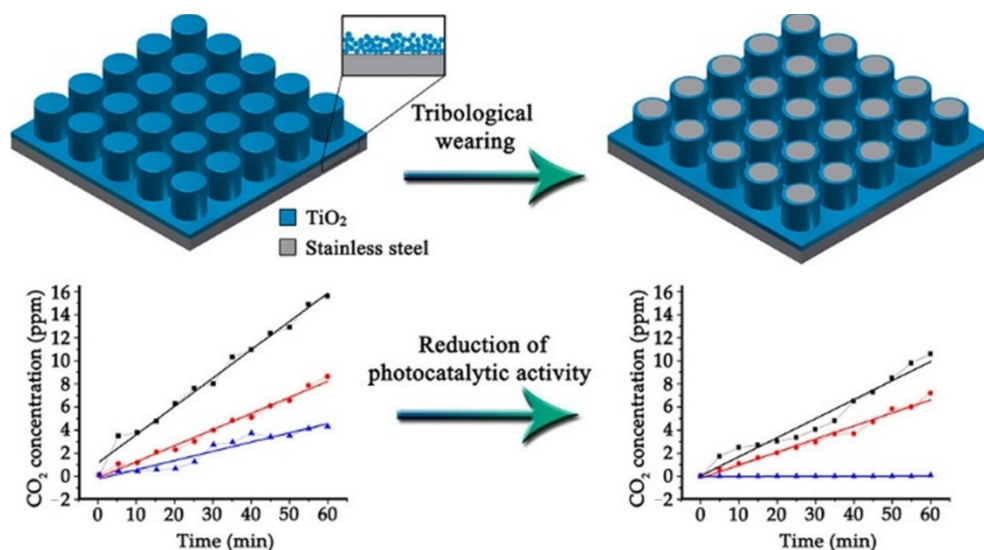


**Figure 5.** Schematic representation of TiO<sub>2</sub> on stainless steel micropillars (top), measured photocatalytic activity of three prepared samples for 1 h (bottom left), and measured photocatalytic activity of three samples after tribological wear (bottom right). (Adapted from [20] Figure 1, with permissions from Elsevier).

## 5. Nanopillars for Photoswitching Achieved by Varying Surface Hydrophobicity and Hydrophilicity

The concept of controlling surface wettability and adhesion of the superhydrophobic surfaces of inorganic oxides has become highly advantageous in biosensing, self-cleaning, solar cells, and liquid–liquid extraction applications. The controlled wettability of these material surfaces influences photoresponsivity because of transitions between the bistable states of inorganic oxides including titanium dioxide, zinc oxide, and tungsten oxide. As a result of UV light exposure, the hole diffusion rate to titanium dioxide surface increases, leaving the titanium–oxygen bonds within the lattice extremely weak and available for increased interaction and hydration with water molecules, thus increasing surface hydrophilicity. Hoshian et al. report the results of three photo/thermal switching processes after measuring the titanium dioxide micropillar overhang geometry and surface nanostructuring while controlling UV exposure time [21]. The test samples include a flat substrate, simple micropillars, micropillars with overhang, flat nanostructured surface, simple micropillar with nanostructures, and a micro/nanostructured overhang sample. The results regarding the three photoswitching processes of rolling to sticky superhydrophobic states, superhydrophobic to hydrophilic states, and superhydrophobic to superhydrophilic states after 1, 5, and 10 min of UV exposure yield slow switching speeds, which remain impractical for applications (Figure 6). The reported photoswitching properties of titanium dioxide indicate that reversible switching from rolling to sticky superhydrophobic states requires only 1 min of UV exposure, due to the photoactive titanium dioxide thin film and overhang geometry of the nanopillars. Quantitative data were not provided in comparison of the samples. The application of TiO<sub>2</sub> thin film and overhang geometry micropillars presents a novel approach to speeding the wetting transition from rolling to sticky superhydrophobic states and improving photoswitching properties.

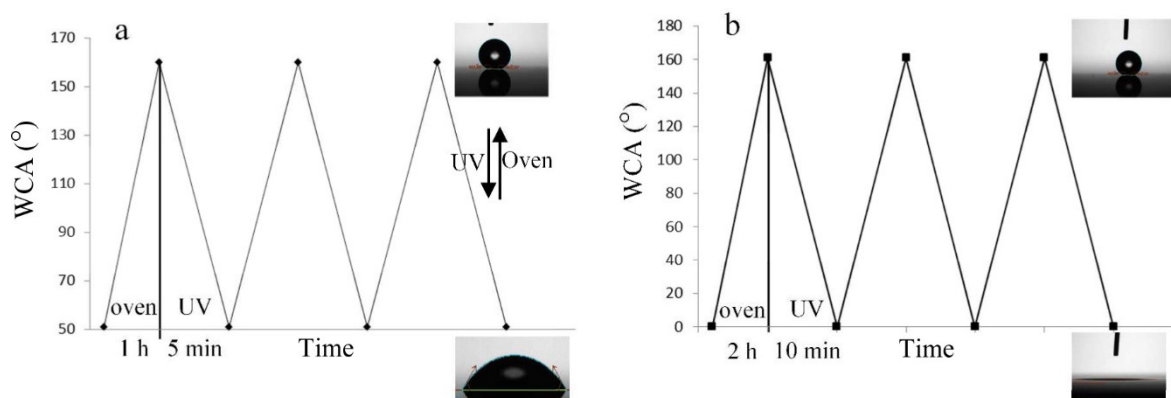


**Figure 6.** (a) Hydrophilic to superhydrophobic transitions by 1 h annealing in oven at 60 °C and 5 min of UV exposure; (b) superhydrophilic to superhydrophobic transitions by 2 h annealing in oven at 60 °C and 10 min of UV exposure. (Adapted from [21] Figure 4, with permissions from ACS).

## 6. Nanopillars for Photocatalytic Soot Oxidation

The generation of TiO<sub>2</sub> radicals capable of oxidizing soot pollutant particles has been confirmed. Recently, Kameya et al. explored the effect of microstructure of TiO<sub>2</sub> on soot oxidation rate by measuring photon absorption of plain substrate (Figure 7) at varying thicknesses and micropillar substrate [22]. The study reports nonlinear increase in electron–hole generation, photon absorption, and soot oxidation rate as a function of increasing plain TiO<sub>2</sub> substrate thickness (<2.5 μm). Two samples were produced for comparison, both TiO<sub>2</sub> microstructures on plain or micropillared substrates. Additionally, the incorporation of TiO<sub>2</sub> nanopillars enhanced photon absorption through multiple scattering, resulting in increased rates of soot removal/oxidation with increasing substrate thickness. The



application of TiO<sub>2</sub> nanopillar substrate, as well as instituting increased film thickness, presents an efficient alternative for environmental repair of soot removal from air particles.

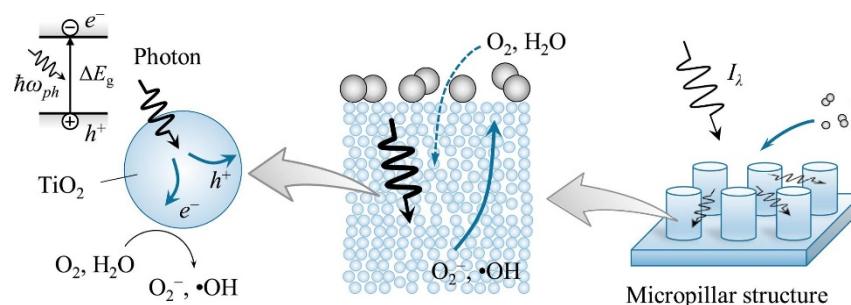


**Figure 7.** Schematic of the multiscale phenomena occurring in the photocatalytic soot oxidation on TiO<sub>2</sub> microstructured substrate. (Adapted from [22] with permissions from Elsevier).

### 7. Nanopillars for Photothermalization

The harvesting of high energy and nonequilibrium “hot” electrons represents a recent application of metal nanostructures with the focus of analyzing photocatalytic activity and the correspondence of electronic structural and optical properties within specific metals.

Hogan and Sheldon [23] investigated the photothermalization dynamics of copper “hot” electrons during continuous wave (CW) optical excitation. Two samples for comparison are gold (Au) and copper (Cu) nanostructures with differing hot electron temperature and lifespan measurements. They reported a considerable abundance, high reactivity, and large steady state population of “hot” electrons in copper, compared to gold and silver (Figure 8). The implementation of copper, rather than gold, metal nanostructures presents a powerful application for plasmonic “hot” electrons in enhancing photocatalytic and photochemical performance, as a result of the characteristically large population of “hot” electrons and the decreased electron lifetime in copper. The kinetic energy measurement of these “hot” electrons provides insight to the photochemical properties of metals, especially copper, silver, and gold; this plasmonic system is applicable to the process of water splitting, carbon dioxide reduction, and ammonia generation.

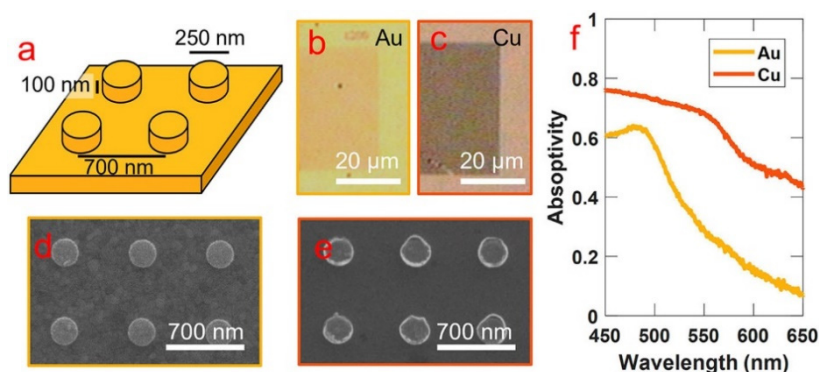


**Figure 8.** (a) A schematic of the fabricated nanostructure with a pitch of 700 nm, a height of 100 nm, and a cylinder diameter of 250 nm on top of a thin film with thickness of 150 nm. Optical and SEM images of the nanostructure are shown in (b,d) for gold and (c,e) for copper, respectively. (f) The absorptivity of the two nanostructures. (Reproduced from [23] Figure 1, with permissions from AIP).

### 8. Nanopillars for Conversion of Carbon Dioxide to Energy—Increasing Photosynthetic Efficiency through Doping of InP Nanopillars with TiO<sub>2</sub>

As an environmentally conscious area of study receiving recent attention in response to the increasing levels of carbon dioxide in the atmosphere, the artificial synthesis technique converting carbon dioxide into hydrocarbon structures, such as methanol and formaldehyde, with semiconductor nanopillars has gained traction. The optimal band gap region

of the semiconductor required for photoreduction is reported as 1.2–1.4 eV, with the additional necessity for proximity of electron affinity of semiconductor and carbon dioxide redox potential. For effective photoreduction, the surface recombination rate of photon-induced electron–hole pairs must remain low [24]. Qiu et al. utilized TiO<sub>2</sub>-passivated Tin-Phosphide (InP) nanopillars to investigate carbon dioxide reduction to methanol under 532 nm illumination within aqueous medium; the study measures methanol production as a function of InP sample preparation—with and without the titanium dioxide-passivated layers and copper cocatalyst nanoparticles (Figure 9)—using high resolution transmission electron microscopy (HRTEM). They reported enhancement of photoconversion efficiency following the incorporation of oxygen vacancies in titanium dioxide by atomic layer deposition; The application of TiO<sub>2</sub>-doped InP nanopillars in carbon dioxide reduction showed an increased Faraday efficiency (8.7%) of methanol production and allows for an 8-fold increase in the performance of this artificial photosynthetic pathway.

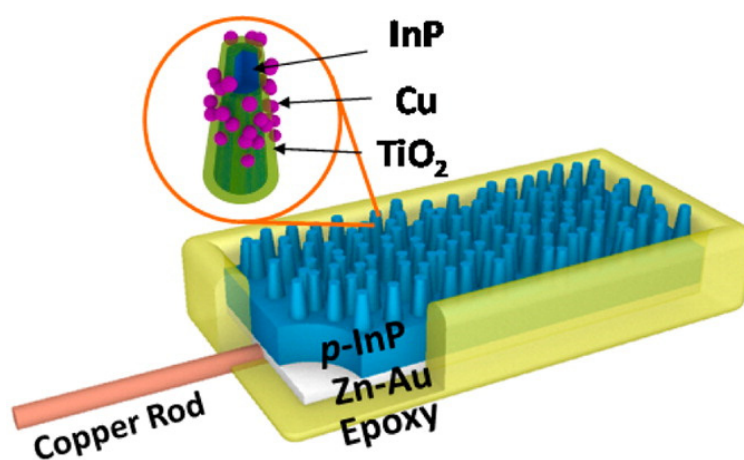


**Figure 9.** Schematic diagram of TiO<sub>2</sub>-passivated InP nanopillars with Cu cocatalyst nanoparticles. (Adapted from [24] Figure 1, with permissions from ACS).

## 9. Conclusions

In summary, this review analyzed the improvement of photocatalytic performance of vertical nanopillar arrays of a variety of photocatalysts, including catalyst in the presence of metal and nonmetal dopants and lattice defects at catalytic interfaces.

Applications of photocatalyst nanopillars have been considered in the context of water splitting, removing organic pollutants from atmospheric and aqueous environments, photoswitching of hydrophobic and hydrophilic surfaces, and energy harnessing through carbon dioxide catabolism; an overall improvement to nanopillar photocatalytic efficiency is achieved through doping with metals and nonmetals, increasing surface area with nanopillar and nanowire structures and introducing lattice defects at catalytic interfaces.

**Author Contributions:** Conceptualization, J.L.W. and J.H.; methodology, J.L.W., J.H. and H.J.; writing—original draft preparation, J.L.W. and J.H.; writing—review and editing, J.L.W., J.H. and H.J.; supervision, H.J. All authors have read and agreed to the published version of the manuscript.

**Funding:** This research received no external funding.

**Institutional Review Board Statement:** Not applicable.

**Informed Consent Statement:** Not applicable.

**Data Availability Statement:** No new data were created or analyzed in this study.

**Conflicts of Interest:** The authors declare no conflict of interest.

## References

1. Kertmen, A.; Barbé, E.; Szkoda, M.; Siuzdak, K.; Babačić, V.; Torruella, P.; Iatsunskyi, I.; Kotkowiak, M.; Rytel, K.; Estradé, S.; et al. Photoelectrochemically Active N-Adsorbing Ultrathin TiO<sub>2</sub> Layers for Water-Splitting Applications Prepared by Pyrolysis of Oleic Acid on Iron Oxide Nanoparticle Surfaces under Nitrogen Environment. *Adv. Mater. Interfaces* **2018**, *1801286*. [[CrossRef](#)]
2. Shuang, S.; Lv, R.; Xie, Z.; Zhang, Z. Surface Plasmon Enhanced Photocatalysis of Au/Pt-decorated TiO<sub>2</sub> Nanopillar Arrays. *Sci. Rep.* **2016**, *6*, 26670. [[CrossRef](#)] [[PubMed](#)]
3. Cheng, H.-E.; Lin, C.-Y.; Hsu, C.-M. Fabrication of SnO<sub>2</sub>-TiO<sub>2</sub> core-shell nanopillar-array films for enhanced photocatalytic activity. *Appl. Surf. Sci.* **2017**, *396*, 393–399. [[CrossRef](#)]
4. Gao, H.; Liu, C.; Jeong, H.E.; Yang, P. Plasmon-Enhanced Photocatalytic Activity of Iron Oxide on Gold Nanopillars. *ACS Nano* **2011**, *6*, 234–240. [[CrossRef](#)] [[PubMed](#)]
5. Zhang, K.-Z.; Lin, B.-Z.; Chen, Y.-L.; Xu, B.-H.; Pian, X.-T.; Kuang, J.-D.; Li, B. Fe-doped and ZnO-pillared titanates as visible-light-driven photocatalysts. *J. Colloid Interface Sci.* **2011**, *358*, 360–368. [[CrossRef](#)]
6. Lalhriatpuia, C.; Tiwari, A.; Shukla, A.; Tiwari, D.; Lee, S.-M. Nanopillars TiO<sub>2</sub> thin film photocatalyst application in the remediation of aquatic environment. *Korean J. Chem. Eng.* **2016**, *33*, 3367–3373. [[CrossRef](#)]
7. Mirabedini, P.S.; Truskowska, A.; Ashby, D.Z.; Rao, M.P.; Greaney, P.A. Coupled Light Capture and Lattice Boltzmann Model of TiO<sub>2</sub> Micropillar Array for Water Purification. *MRS Adv.* **2019**, *4*, 2689–2698. [[CrossRef](#)]
8. Pavlenko, M.; Siuzdak, K.; Coy, E.; Załęski, K.; Jancelewicz, M.; Iatsunskyi, I. Enhanced solar-driven water splitting of 1D core-shell Si/TiO<sub>2</sub>/ZnO nanopillars. *Int. J. Hydrog. Energy* **2020**, *45*, 26426–26433. [[CrossRef](#)]
9. Liao, A.; He, H.; Tang, L.; Li, Y.; Zhang, J.; Chen, J.; Chen, L.; Zhang, C.; Zhou, Y.; Zou, Z. Quasi-Topotactic Transformation of FeOOH Nanorods to Robust Fe<sub>2</sub>O<sub>3</sub> Porous Nanopillars Triggered with a Facile Rapid Dehydration Strategy for Efficient Photoelectrochemical Water Splitting. *ACS Appl. Mater. Interfaces* **2018**, *10*, 10141–10146. [[CrossRef](#)]
10. Xing, Z.; Li, Z.; Wu, X.; Wang, G.; Zhou, W. In-situ S-doped porous anatase TiO<sub>2</sub> nanopillars for high-efficient visible-light photocatalytic hydrogen evolution. *Int. J. Hydrog. Energy* **2016**, *41*, 1535–1541. [[CrossRef](#)]
11. Qu, Y.; Zhou, W.; Ren, Z.; Tian, C.; Li, J.; Fu, H. Heterojunction Ag-TiO<sub>2</sub> Nanopillars for Visible-Light-Driven Photocatalytic H<sub>2</sub> Production. *ChemPlusChem* **2014**, *79*, 995–1000. [[CrossRef](#)]
12. Ahn, H.-J.; Yoon, K.-Y.; Kwak, M.-J.; Jang, J.-H. A Titanium-Doped SiO<sub>x</sub> Passivation Layer for Greatly Enhanced Performance of a Hematite-Based Photoelectrochemical System. *Angew. Chem.* **2016**, *128*, 10076–10080. [[CrossRef](#)]
13. Kimura, T.; Yamauchi, Y.; Miyamoto, N. Highly Photoactive Porous Anatase Films Obtained by Deformation of 3D Mesostructures. *Chem. Eur. J.* **2011**, *17*, 4005–4011. [[CrossRef](#)] [[PubMed](#)]
14. Song, J.-H.; Sonkaria, S.; Lee, B.; Kim, Y.G.; Ahn, S.-H.; Lee, C.S.; Khare, V. Tuning Intercrystalline Void-like Defects in Nanowire Clusters to TiO<sub>2</sub> Quantum Wires with Enhanced Photocatalytic Performance. *ACS Appl. Energy Mater.* **2019**, *2*, 5643–5655. [[CrossRef](#)]
15. Shuang, S.; Zhang, Z. The Effect of Annealing Treatment and Atom Layer Deposition to Au/Pt Nanoparticles-Decorated TiO<sub>2</sub> Nanorods as Photocatalysts. *Molecules* **2018**, *23*, 525. [[CrossRef](#)]
16. Tiwari, A.; Shukla, A.; Lalliansanga; Tiwari, D.; Lee, S.-M. Au-nanoparticle/nanopillars TiO<sub>2</sub> meso-porous thin films in the degradation of tetracycline using UV-A light. *J. Ind. Eng. Chem.* **2019**, *69*, 141–152. [[CrossRef](#)]
17. Jiang, W.; Ullah, N.; Divitini, G.; Ducati, C.; Kumar, R.V.; Ding, Y.; Barber, Z.H. Vertically Oriented TiO<sub>x</sub>N<sub>y</sub> Nanopillar Arrays with Embedded Ag Nanoparticles for Visible-Light Photocatalysis. *Langmuir* **2012**, *28*, 5427–5431. [[CrossRef](#)]
18. Shuang, S.; Xie, Z.; Zhang, Z. Enhanced photocatalytic properties of CdS nanoparticles decorated α-Fe<sub>2</sub>O<sub>3</sub> nanopillar arrays under visible light. *J. Colloid Interface Sci.* **2017**, *494*, 107–113. [[CrossRef](#)]
19. Nissilä, T.; Sainiemi, L.; Karikko, M.-M.; Kemell, M.; Ritala, M.; Franssila, S.; Kostianen, R.; Ketola, R.A. Integrated photocatalytic micropillar nanoreactor electrospray ionization chip for mimicking phase I metabolic reactions. *Lab Chip* **2011**, *11*, 1470–1476. [[CrossRef](#)]
20. Temerov, F.; Ammosova, L.; Haapanen, J.; Mäkelä, J.M.; Suvanto, M.; Saarinen, J.J. Protective stainless steel micropillars for enhanced photocatalytic activity of TiO<sub>2</sub> nanoparticles during wear. *Surf. Coat. Technol.* **2020**, *381*, 125201. [[CrossRef](#)]
21. Hoshian, S.; Jokinen, V.P.; Hjort, K.; Ras, R.H.; Franssila, S. Amplified and Localized Photoswitching of TiO<sub>2</sub> by Micro- and Nanostructuring. *ACS Appl. Mater. Interfaces* **2015**, *7*, 15593–15599. [[CrossRef](#)] [[PubMed](#)]
22. Kameya, Y.; Torii, K.; Hirai, S.; Kaviany, M. Photocatalytic soot oxidation on TiO<sub>2</sub> microstructured substrate. *Chem. Eng. J.* **2017**, *327*, 831–837. [[CrossRef](#)]
23. Hogan, N.; Sheldon, M. Comparing steady state photothermalization dynamics in copper and gold nanostructures. *J. Chem. Phys.* **2020**, *152*, 061101. [[CrossRef](#)] [[PubMed](#)]
24. Qiu, J.; Zeng, G.; Ha, M.-A.; Ge, M.; Lin, Y.; Hettick, M.; Hou, B.; Alexandrova, A.N.; Javery, A.; Cronin, S.B. Artificial Photosynthesis on TiO<sub>2</sub>-Passivated InP Nanopillars. *Nano Lett.* **2015**, *15*, 6177–6181. [[CrossRef](#)] [[PubMed](#)]